DOI: https://doi.org/10.1007/978-981-4585-86-6_9-2

Numerical Modelling of Pulverised Coal Combustion

Zhao F. Tian[*], *Peter J. Witt*[+], *M. Philip Schwarz*[+] *and William Yang*[+]

* zhao.tian@adelaide.edu.au

School of Mechanical Engineering

The University of Adelaide

SA 5005 Australia

[+] CSIRO, Mineral Resources Flagship

ABSTRACT

Many thermal power generation plants rely on combustion of pulverised coal carried out in large furnaces. Design and improvement of these furnaces can be effectively assisted by using numerical modelling with Computational Fluid Dynamics (CFD) techniques to develop a detailed picture of the conditions within the furnace, and the effect of operating conditions, coal type, and furnace design on those conditions. The equations governing CFD models of pulverised coal combustion are described, with a focus on sub-models needed for devolatilisation, combustion and heat transfer. The use of the models is discussed with reference to examples of CFD modelling of brown coal fired furnaces in the Latrobe Valley in Australia and black coal fired furnaces described in the literature. Extensions to the CFD models that are required to tackle specific industrial and environmental issues are also described. These issues include control of NOx and SOx emissions and the effect of slagging and fouling on furnace and boiler operation.

KEY WORDS: CFD, coal combustion, tangentially fired, drying model, devolatilisation model, char combustion model, NOx, Soot model, turbulence model

1. INTRODUCTION

Coal-fired electricity generation is still dominant in the power industries of many countries, despite the rapid increase of renewable electricity generation in recent years. In 2010, coal-fired electricity generation accounted for 40% of the electricity generation worldwide (EIA 2013). In Australia, coal including black coal and brown coal generated about 64% of electricity in 2012-2013 (BREE 2014). It is particularly noteworthy that in the state of Victoria, brown coal from the Latrobe Valley region produces over 85% of the state's electricity supply (Allardice 2000). Pulverised coal (PC) combustion is one of the major technologies for the conversion of chemical energy in coal into electricity. In the brown coal fired power plants in the Latrobe Valley, all existing boilers use PC combustion technologies.

With advances in computing power and modelling techniques, computational fluid dynamics (CFD) has evolved into a feasible tool for scientists and engineers who can apply it to better understand PC combustion in furnaces (Tian et al. 2009) and therefore optimise the design and operation of PC boilers. Nevertheless, PC combustion in furnaces is one of the most difficult processes to model mathematically, since it generally involves the simultaneous coupled processes of three-dimensional gas-particle fluid dynamics, turbulent mixing, heat transfer, and complex homogeneous and heterogeneous chemical reaction kinetics (Viskanta and Mengüç 1987). In modelling real industrial installations, additional complications arise from slagging and fouling of heat transfer surfaces, variability in feed characteristics and inevitable uncertainties in actual structural geometry due, for example, to occasional damage or maintenance issues.

Figure 1 shows the major physical and chemical processes that occur during the burning of pulverised coal particles in a tangentially-fired PC furnace. Fine coal particles, pulverised in mills, are blown into the furnace through a number of burners. Once the particles enter the furnace, they are heated by hot furnace gases and radiation from the flame, they start to dry when their temperature reaches about 100-110°C (Wu 2005). When the particles are heated further to a certain critical temperature (depending on the coal type and size), devolatilisation starts and volatiles are released from the particles. The products of devolatilisation include non-condensable volatiles (light gases), condensable volatiles (tars) and remaining solid particles that normally comprise char and mineral matter. The volatiles react with oxygen from the combustion air and other oxidants in the furnace. Finally char particles react with gases in the furnace, leaving mineral matter and probably a small fraction of unburnt char in the solid

particles. These particles (ash) and the furnace gas flow through convective heat transfer sections such as superheaters, reheaters and economisers, exchanging heat with the working fluid (water/steam) in the convective devices. Typical exhaust gases comprise CO_2, N_2, H_2O, O_2, and small amounts of NO_x, SO_x, CO and particulate matters (PM). After leaving the convective passes exhaust gases will normally go through various air pollution control equipment before being discharged through the stack.

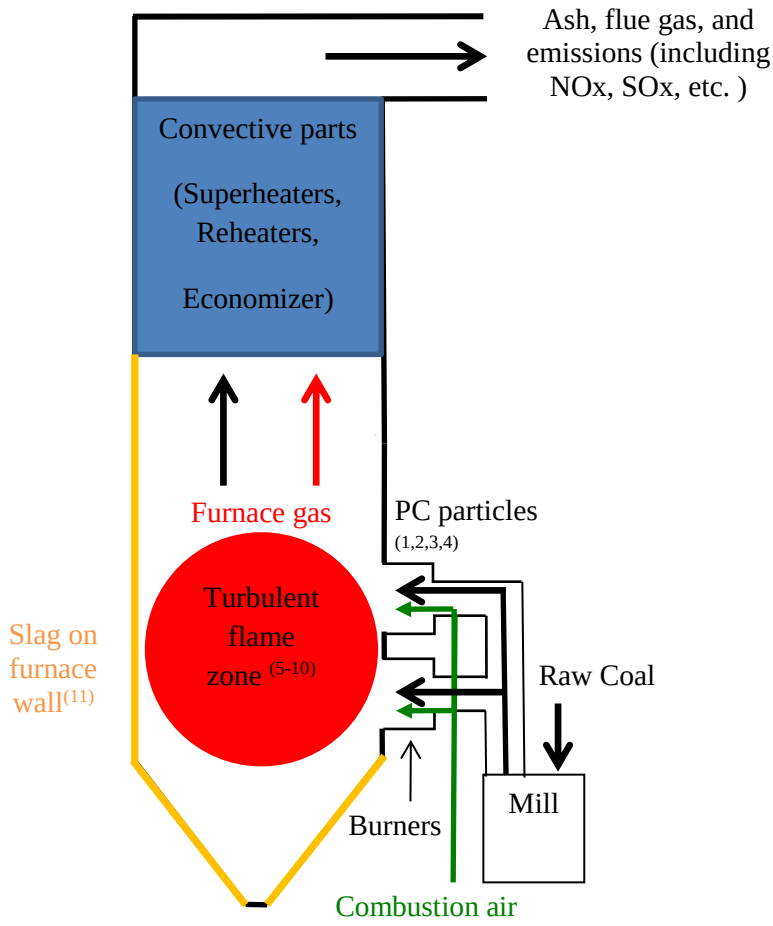

Figure 1. A schematic drawing of PC coal fired furnace and some typical CFD sub-models required to model these processes. Submodels: (1) particle phase model, (2) evaporation/drying model, (3) devolatilisation model, (4) char combustion model, (5) turbulence model, (6) turbulence-reaction interaction model, (7) radiation model, (8) soot model, (9) NOx model, (10) SOx model, (11) slagging model.

In the CFD approach, mathematical descriptions of each of these processes in the furnaces are called ‘sub-models’ because they can be developed and updated in the same way that modules in circuit boards can be replaced (Niksa 1996). As shown in Figure 1, a CFD code for modelling coal combustion probably needs the following sub-models: (1) model for particle phase motion,

(2) evaporation/drying model, (3) devolatilisation model, (4) char combustion model, (5) turbulence model, (6) turbulence-reaction interaction model (gas phase reaction models), (7) radiation model, (8) soot model, (9) NO_x model, (10) SO_x model, (11) slagging model. Figure 2, adapted from Tian et al. (2010a) shows some sub-models available in the commercial CFD code ANSYS/CFX 14.

This book chapter briefly reviews and describes the mathematical equations of some of these sub-models. The authors have implemented some of these sub-models into a CFD model of a tangentially-fired PC furnace at the TRUenergy Yallourn power plant, Latrobe Valley, Australia (Tian et al. 2010a). This CFD model was developed based on the commercial CFD code, ANSYS/CFX. The model has been validated against plant measurements and applied to investigate the effects of several operating conditions at full load, such as different out-of-service firing groups and different combustion air distributions on the coal flames (Tian et al. 2010b). The CFD furnace model was then used to assess the combustion of pre-dried brown coal in the furnace that was designed for raw or non-pre-dried brown coal (Tian et al. 2012). In this book chapter, additional results of the CFD furnace model are reported as examples of the sub-model applications.

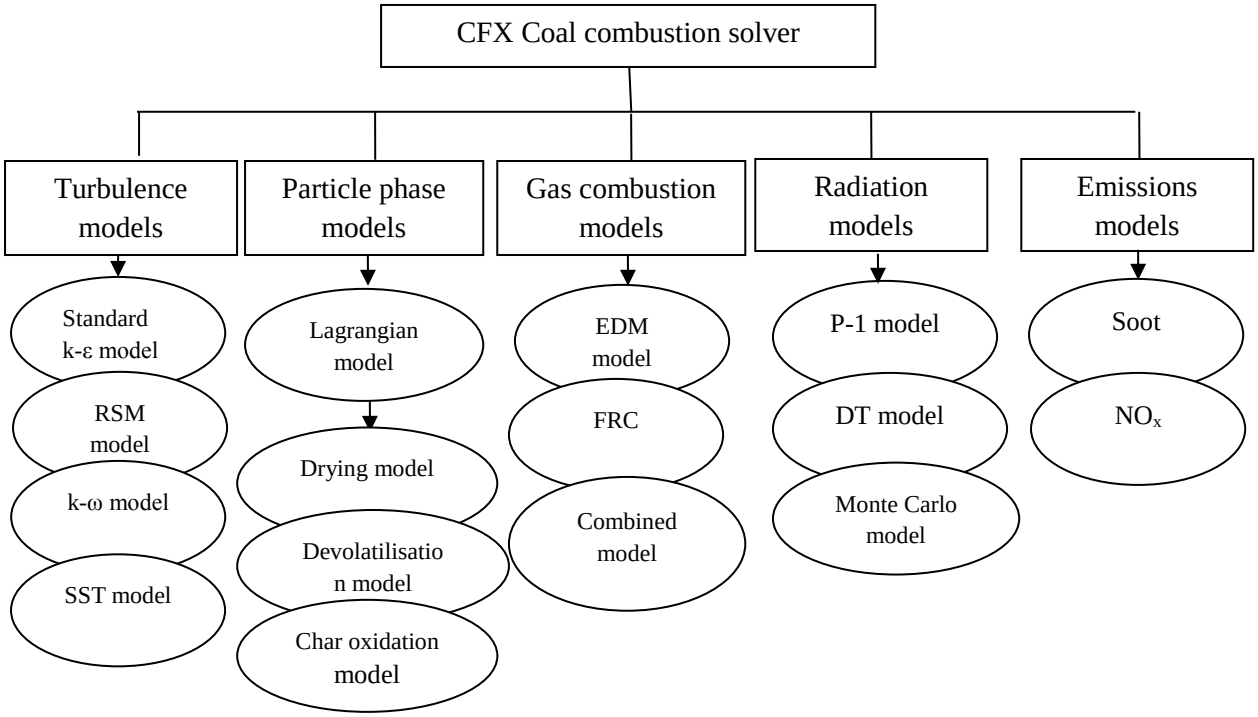

Figure 1. The structure of CFD coal combustion solver, adapted from (Tian et al. 2010a). RSM: Reynolds Stress model; SST: Shear stress transport model; EDM: Eddy dissipation model; FRC: Finite rate chemistry model; Combined model: Combined EDM/FRC model; DT: Discrete transfer model.

2. GAS PHASE MODEL

2.1 Gas phase governing equations

In CFD models of pulverized coal combustion, gases in the furnace are normally considered to be a mixture consisting of the gaseous components, O_2, H_2O, CO_2, CO, N_2, NO, and volatiles (Tian et al. 2010a). Volatiles can be taken as one single gas component, a mixture of light gas and tar, or a mixture of individual gases such as CH_4, C_2H_2, etc. To reduce the computing time, these components are normally assumed to be mixed at the molecular level, hence having the same mean velocity, pressure, temperature and turbulence fields (Tian et al. 2010a). The Navier-Stokes equations are used to solve the continuity and momentum equations of the gas mixture. The gas phase equations solved in ANSYS/CFX are given below as an example of the steady state governing equations for CFD models. Equations 1 and 2 are the continuity equation and momentum equation of the mean steady state after Reynolds averaging:

$$\nabla \cdot \left(\rho_g U_g\right) = 0 \tag{1}$$

$$\nabla \cdot \left(\rho_g U_g U_g\right) = -\nabla p_g + \nabla \cdot \left\{\mu_g \left[\nabla U_g + \left(\nabla U_g\right)^T\right] - \rho_g \overline{U_g U_g}\right\} + S_M , \tag{2}$$

here U_g is the gas phase mean velocity vector; P_g is the gas phase mean pressure; S_M is the external momentum source such as gravity and forces from the coal particle phase; and ρ_g is the gas mixture density defined as:

$$\rho_g = \sum_{I=1}^{Nc} Y_I \rho_I , \tag{3}$$

where ρ_I is the mass density of the component I. N_c is the number of modelled species in the gas mixture, and Y_I is the mass fraction of the species I, solved by the following equation:

$$\nabla \cdot \left(\rho_g U_g Y_I\right) = \nabla \cdot \left(\Gamma_{I.eff} \nabla Y_I\right) + S_I \tag{4}$$

In this equation, S_I is the source term of the species related to generation or destruction of the species by reaction. Other properties of the gas mixture, such as the gas mixture molecular viscosity μ_g and the gas mixture specific heat capacity at constant pressure $C_{p,g}$, are calculated in the same manner as Equation 3:

$$\alpha_g = \sum_{I=1}^{Nc} Y_I \alpha_I , \tag{5}$$

where α_g in the gas mixture property being considered.

The effective diffusion coefficient of species I, $\Gamma_{I.eff}$, in Equation 4 is defined as:

$$\Gamma_{I.eff} = \Gamma_I + \frac{\mu_t}{Sc_t}, \tag{6}$$

Where Γ_I is the molecular diffusion coefficient of species, $\Gamma_I = \rho_I D_I$, here D_I is the kinematic diffusivity of the species I. Sc_t is the turbulent Schmidt number and μ_t is turbulent viscosity.

The source term S_I in Equation 4 is due to chemical reaction involving the species. There is one transport equation of each gas component except the constraint gas N_2. The mass fraction of N_2 is calculated by using the following equation:

$$\sum_{I=1}^{Nc} Y_I = 1 \tag{7}$$

The Reynolds averaged energy equation for the gas mixture can be:

$$\nabla \cdot \left(\rho_g U_g h_g\right) = \nabla \cdot \left(\lambda_g \nabla T_g + \frac{\mu_t}{\mathrm{Pr}_t} \nabla h_g \right) + S_E, \tag{8}$$

where h_g is the gas mixture enthalpy. Pr_t is the turbulent Prandtl number. The energy source term S_E includes thermal energy from chemical reactions and thermal radiative heat transfer.

In most CFD coal combustion models, the Reynolds averaged Navier Stokes (RANS) modelling approach is used to handle turbulence. In RANS models, the Reynolds stresses terms $-\rho_g \overline{U_g U_g}$ in the momentum Equation 2 are modeled based on the Boussinesq hypothesis:

$$-\rho_g \overline{U_g U_g} = \mu_t \left[\nabla U_g + \left(\nabla U_g\right)^T\right] - \frac{2}{3}\delta_{ij}\left(\rho_g k_g + \mu_t \nabla \cdot U_g\right), \tag{9}$$

where μ_t is the turbulence viscosity that can be calculated by applying turbulence models that will be discussed later. δ_{ij} is the Kronecker delta that is 1 when i=j and 0 when i≠j.

2.2 Turbulence models

Turbulent mixing is one of the major factors controlling the local proportions of fuel and oxygen throughout the primary flame zones and thereby exerting a predominant effect on heat

release rates, heat fluxes onto steam tubes, carbon burnout times and pollutant formation rates (Niksa 1996). In CFD techniques, turbulence models are used to close the equations for the fluctuating quantities and thereby include the effects of eddies on the time averaged flow.

The Reynolds stresses in Equation 9 can be also directly calculated from six transport equations and this is called the Reynolds Stress model (RSM). The RSM is a second order RANS model but has been used to predict coal combustion by only a few researchers such as Weber et al. (1995) and Zhang and Nieh (1997). The RSM has been shown to perform better than *k*-*ε* models in predicting of isothermal swirl jets (German and Mahmud 2005; Weber et al. 1990) due to two equation models not being able to reliably resolve flows with strong streamline curvatures. This limitation of two equations models can be partly overcome by a curvature correction term to the turbulence production term. However work at International Flame Research Foundation (IFRF) (Weber et al. 1995) demonstrated that this advantage of the RSM over *k*-*ε* models was not found in the burning jet applications (Niksa 1996). Backreedy et al. (2006) found that the performance of RSM in modelling a swirl coal flame in a pilot-scale furnace is not better than that of *k*-*ε* models. This is confirmed by a recent modelling project that compared the performance of several RANS models in modelling swirling flow in a vortex flow reactor (Tian et al. 2015). The BSL RSM can predict the anisotropic Reynolds stresses that the SST model and the standard *k*-*ε* model cannot predict, but this does not make it more accurate in predicting the mean flow-field than the other two models. Application of the RSM requires more computational resources than is required by the standard *k*-*ε* and similar first order models, partially due to the need to solve additional transport equations of the Reynolds Stresses and probably due to the poor convergence characteristics and stability of RSM.

The standard *k*-*ε* model is commonly applied in studies of coal combustion in furnaces. For the standard *k*-*ε* model the turbulent viscosity, μ_t, in Equation 8 is computed from:

$$\mu_t = C_\mu \rho_g k_g^2 / \varepsilon_g \tag{10}$$

where k_g is the turbulence kinetic energy of the gas mixture and ε_g is the kinetic energy dissipation rate of the gas mixture. In the standard *k*-*ε* model, the turbulence kinetic energy and the kinetic energy dissipation rate of the gas mixture are calculated by solving two transport equations.

The turbulence kinetic energy equation for the standard *k*-*ε* model is:

$$\nabla \cdot \left(\rho_g U_g k_g\right) = \nabla \cdot \left[\left(\mu_g + \frac{\mu_t}{\sigma_k}\right)\nabla k_g\right] + P_k - \rho_g \varepsilon_g \tag{11}$$

Here, the rate of production of turbulence kinetic energy P_k is modeled by:

$$P_k = \mu_t \nabla U_g \cdot \left(\nabla U_g + (\nabla U_g)^T\right) - \frac{2}{3}\nabla \cdot U_g \left(\mu_t \nabla \cdot U_g + \rho_g k_g\right) \tag{12}$$

The kinetic energy dissipation rate equation is:

$$\nabla \cdot \left(\rho_g U_g \varepsilon_g\right) = \nabla \cdot \left[\left(\mu_g + \frac{\mu_t}{\sigma_\varepsilon}\right)\nabla \varepsilon_g\right] + \frac{\varepsilon_g}{k_g}(C_{\varepsilon 1} P_k - C_{\varepsilon 2}\rho_g \varepsilon_g) \tag{13}$$

The values of the constants are C_μ = 0.09, σ_k = 1.0, σ_ε = 1.3, $C_{1\varepsilon}$ = 1.44, $C_{2\varepsilon}$ = 1.92 (Launder and Spalding 1974).

Compared to the RSM, the standard *k-ε* model is less computationally intensive while providing a similar level of predictive accuracy to the RSM for most coal combustion applications not involving strong swirling flow fields. The standard *k-ε* model has been used to simulate coal flames in pilot-scale furnaces (Tian et al. 2010a), e.g. Lockwood and Salooja (1983), Truelove and Holcombe (1991), Zhou et al. (2002) and many others, and full scale furnaces by workers such as Belosevic et al. (2006) and Xu et al. (2001).

One of the major shortcomings of the standard *k-ε* model is that it cannot predict the adverse pressure gradient properly; the standard *k-ε* model significantly over-predicts shear stress levels and thereby delays separation (Menter 1992). Another shortcoming relates to the numerical stiffness of the equations when integrated through the viscous sublayer (Menter 1992). Many modified *k-ε* models have been derived from the standard *k-ε* model in order to overcome these shortcomings, one of which is the Re-Normalization Group (RNG) *k-ε* model that has been used in coal combustion modelling. The transport equations for gas phase k_g and ε_g in the RNG *k-ε* model are given as follows:

$$\nabla \cdot \left(\rho_g U_g k_g\right) = \nabla \cdot \left[\left(\mu_g + \frac{\mu_t}{\sigma_{k,RNG}}\right)\nabla k_g\right] + P_k - \rho_g \varepsilon_g \tag{14}$$

$$\nabla \cdot \left(\rho_g U_g \varepsilon_g\right) = \nabla \cdot \left[\left(\mu_g + \frac{\mu_t}{\sigma_{\varepsilon,RNG}}\right)\nabla \varepsilon_g\right] + \frac{\varepsilon_g}{k_g}(C_{\varepsilon 1,RNG} P_k - C_{\varepsilon 2,RNG}\rho_g \varepsilon_g) \tag{15}$$

$C_{\varepsilon 1,RNG}$ is calculated as:

$$C_{\varepsilon 1,RNG} = 1.42 - f_\eta \ , \tag{16}$$

where

$$f_\eta = \frac{\eta\left(1-\frac{\eta}{4.38}\right)}{(1+\beta_{RNG}\eta^3)} \tag{17}$$

$$\eta = \sqrt{\frac{P_k}{\rho_g C_{\mu,RNG}\varepsilon_g}} \tag{18}$$

and where β_{RNG} is 0.012.

The values of the other constants are $C_{\mu,RNG}$ = 0.0845, $\sigma_{k,RNG}$ = 0.7179, $\sigma_{\varepsilon,RNG}$ = 0.7179, $C_{\varepsilon 2,RNG}$ = 1.68 (Versteeg and Malalasekera 2007).

The Re-Normalisation Group (RNG) *k-ε* model has been used in some coal combustion modelling projects. Fan et al. (2001) compared modeling results from the RNG *k-ε* model and the standard *k-ε* model in a tangentially fired furnace against experimental data, and found the RNG *k-ε* model gave better results for swirling flow and sharper flow gradients within calculated regions than the standard *k-ε* model. Backreedy et al. (2006) used the RNG *k-ε* model in a coal test furnace model, as the RNG *k-ε* model is believed to have advantages over the standard *k-ε* model in swirling flows. Nevertheless, these advantages of the RNG *k-ε* model over the standard *k-ε* model in swirling flows have been a matter of some controversy (Saqr 2011).

The Wilcox *k-ω* model (Wilcox 1988), Menter *k-ω* model that also called Baseline (BSL) model, and Shear-stress transport (SST) model (Menter 1994) are another class of two-equation RANS models. The SST model is a hybrid approach between the standard *k-ε* model and the *k-ω* model. In the SST model, in the region near walls, the *k-ω* model is used as it performs well for near wall flows and can avoid the use of wall functions also it allows the accurate specification of ω values on the wall surface hence avoiding issues of defining ε near wall for fine grids. In the region far away from wall, the standard *k-ε* model is used as it is robust in the free stream while *k-ω* model is sensitive to the free stream value of ω (Versteeg and Malalasekera 2007).

The transport equations of k_g and ω_g in the SST model are shown below, with $\omega_g=\varepsilon_g/k_g$. The transport equations of k_g and ω_g of the SST model are:

$$\nabla\cdot\left(\rho_g U_g k_g\right) = \nabla\cdot\left[\left(\mu_g + \frac{\mu_t}{\sigma_{k3}}\right)\nabla k_g\right] + P_k - \beta'\rho_g k_g \omega_g \tag{19}$$

$$\nabla\cdot\left(\rho_g U_g \omega_g\right)=\nabla\cdot\left[\left(\mu_g+\frac{\mu_t}{\sigma_{\omega 3}}\right)\nabla\omega_g\right]+\alpha_3\frac{\omega_g}{k_g}P_k+(1-F_1)2\rho_g\frac{1}{\sigma_{\omega,2}\omega_g}\nabla\omega_g\nabla k_g-\beta_3\rho_g\omega_g^2 \tag{20}$$

The turbulent viscosity, μ_t, is calculated as:

$$\mu_t=\frac{\rho_g k_g \alpha_1}{\max(\alpha_1\omega_g, SF_2)}, \tag{21}$$

where $S=\sqrt{2S_{ij}S_{ij}}$.

The blending function F_1 in Equation 20 is calculated as:

$$F_1=\tanh\left(\arg_1^4\right),\ \arg_1=\min\left[\max\left(\frac{\sqrt{k_g}}{0.09\omega_g y},\frac{500\mu_g}{\rho_g y^2\omega_g}\right),\frac{4\rho_g k_g}{\sigma_{\omega,2}D_\omega^+ y^2}\right]$$

$$D_\omega^+=\max\left[2\rho_g\frac{1}{\sigma_{\omega,2}}\frac{1}{\omega_g}\nabla k_g\nabla\omega_g, 10^{-10}\right] \tag{22}$$

where y is the distane to the nearest wall. The blending function F_2 in Equation 21 is given as:

$$F_2=\tanh\left(\arg_2^2\right),\quad \arg_2=\max\left(\frac{2\sqrt{k_g}}{0.09\omega_g y},\frac{500\mu_g}{\rho_g y^2\omega_g}\right) \tag{23}$$

The values of the constants employed in the SST model are β'=0.09, α_1=5/9, α_3=0.44, β_3=0.0828, $\sigma_{\omega,2}$=1/0.856 (Versteeg and Malalasekera 2007).

Only a few studies of coal combustion using the *k-ω* or the SST model can be found in the literature. In a CFD modelling study (Tian et al. 2009), six first order RANS models , namely, the standard *k-ε* model, a modified *k-ε* model, RNG *k-ε* model, Wilcox *k-ω* model, BSL *k-ω* model and SST models were used to simulate a non-swirling coal flame in a pilot-scale furnace of IFRF. The standard *k-ε* model, RNG *k-ε* model, BSL and SST models were found to be generally in good agreement with the experimental data. Predictions using the SST model and BSL *k-ω* model were almost identical, and results of the standard *k-ε* model and the RNG *k-ε* model were similar (Tian et al. 2010b). The SST model and the standard *k-ε* model were further tested in modelling an isothermal gas-particle flow in three inclined rectangular jets in crossflow (Tian et al. 2011). The flow configuration and flow conditions were scaled based on typical flow conditions experienced in the Victorian brown coal furnace burners (Tian et al. 2010a). Gas and particle flows predicted by both models were found to be in reasonable

agreement with the detailed experimental data, although the SST model showed a slightly better agreement with the measurements than the standard *k*-*ε* model (Tian et al. 2010a). The SST and the standard *k*-*ε* model were then employed in a CFD model of a 375 MW tangentially fired furnace (Tian et al. 2010a) burning high-moisture brown coal. Both turbulence models provide similar predictions that were in good agreement with the plant data (Tian et al. 2010a).

The standard *k*-*ε* model has been found to perform particularly well in confined flows where Reynolds shear stresses are most important (Versteeg and Malalasekera 2007). In tangentially fired furnaces, the strong vortex at the center formed by the impinging jets from corners or walls greatly increases the turbulence transport in the furnaces (Basu et al. 1999), therefore the flows in the furnaces can be taken as turbulence transport dominated flows. The major advantage of the SST model over the standard *k*-*ε* model is the inclusion of the shear rate magnitude, S, in Equation 21, which ensures the ratio of turbulence production to turbulence dissipation larger than one in adverse pressure gradient flows (Menter 1992). However, this supposed advantage does not appear to result in a clearly better prediction forthe tangentially fired flames, though the separation of flows are indeed found in the furnace as shown in Figure 3. Figure 3a-c show the predicted flow vectors on a horizontal plane at the exit of the upper main burner when firing units 3&6, 5&6 and 2&6 are out of service, respectively. Flow separations can be found in Figure 3 between jets. For example, as shown in Figure 3a, primary gas flows in the furnace as jets and these high speed jets entrain furnace gas and secondary air. This entrainment helps to form recirculations and flow separations. The details of the CFD model and boundary conditions for the cases shown in Figure 3 can be found in previous papers (Tian et al. 2010a; Tian et al. 2010b).

FU4 FU5

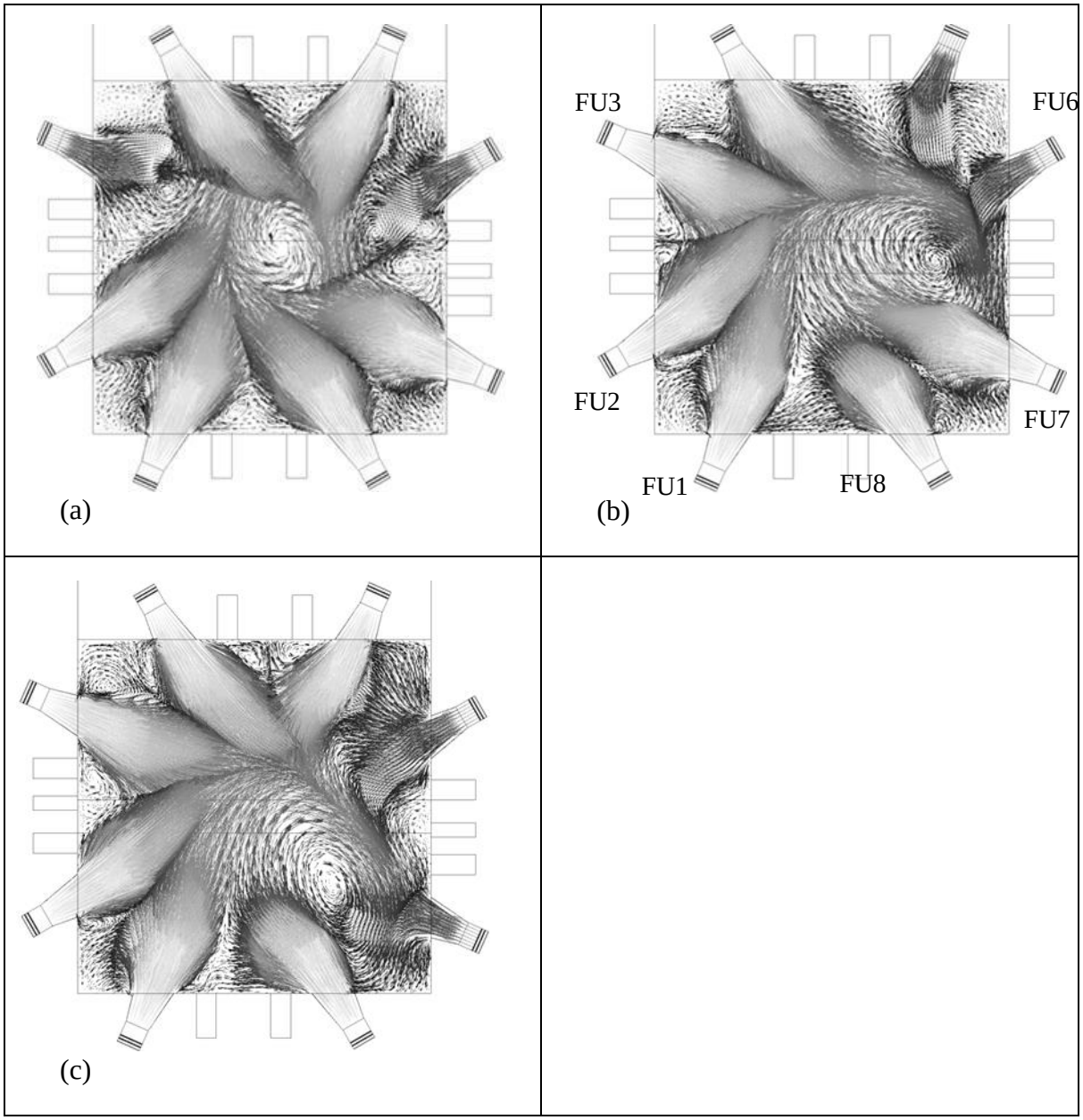

Figure 3 Predicted flow patterns for cases (a) Firing units (FU) 3&6 out-of-service (b) Firing units (FU) 5&6 out-of-service, (c) Firing units (FU) 6&7 out-of-service.

2.3 Gas phase combustion: gas reaction kinetics

The gas phase reactions in coal fired furnaces are very complex. Not all the species and reaction chemistry can be included in the CFD models, partially due to the large computing time required to transport all the species and the stiffness of the large number of intermediate reactions. This problem is further complicated by the heterogeneous nature of coal and the devolatilisation process making knowing the detailed chemical composition of volatiles and subsequent reactions extraordinarily difficult. As discussed in (Yeoh and Yuen 2009), CFD techniques for partial differential equations require computing time roughly proportional to N_s^2

(N_s is the number of species). If all the reaction species found in the PC furnace are included in the CFD model, the computing time will be excessive. Furthermore, except for some simpler alkane hydrocarbon fuels such as CH_4 and C_2H_2, comprehensive reaction chemistry for complex fuel is still not well determined (Yeoh and Yuen 2009). Therefore global reaction schemes are normally used in CFD modelling of the gas phase volatile combustion of coal.

As noted earlier and described in detail below coal combustion consists of a number of stages with a critical stage being the devolatilisation of the solid particle to produce gas phase volatiles:

$$\text{Coal} \rightarrow \text{Volatiles} + \text{C(char)} \tag{24}$$

Volatile combustion can be modeled by the global single step reaction:

$$\text{Volatiles(HC)} + \text{O}_2 \rightarrow \text{CO}_2 + \text{H}_2\text{O} \tag{25}$$

Tian et al. (2010b) notes that the concentration of CO cannot be calculated by the above single step reaction. If understanding the CO concentration is important for the coal combustion modeling work being undertaken, the following reaction scheme was proposed in (Tian et al. 2010b):

$$\text{Coal} \rightarrow \text{Volatiles} + \text{C(char)} \tag{26}$$

$$\text{Volatiles(HC)} + \text{O}_2 \rightarrow \text{CO} + \text{H}_2\text{O} \tag{27}$$

$$\text{C(char)} + \frac{1}{2}\text{O}_2 \rightarrow \text{CO} \tag{28}$$

$$\text{CO} + \frac{1}{2}\text{O}_2 = \text{CO}_2 \tag{29}$$

Figure 4 shows the predicted CO concentration in the furnace of (Tian et al. 2010b) based on the combustion scheme shown above. More species and reactions can be added in the CFD model, however, as mentioned above, the computing time will increase and details of the chemistry are required. When predition of NO_x and/or SO_x emissions is required, the NO_x species and SO_x species can be added to the gas mixture. NO_x and SO_x models are briefly reviewed later.

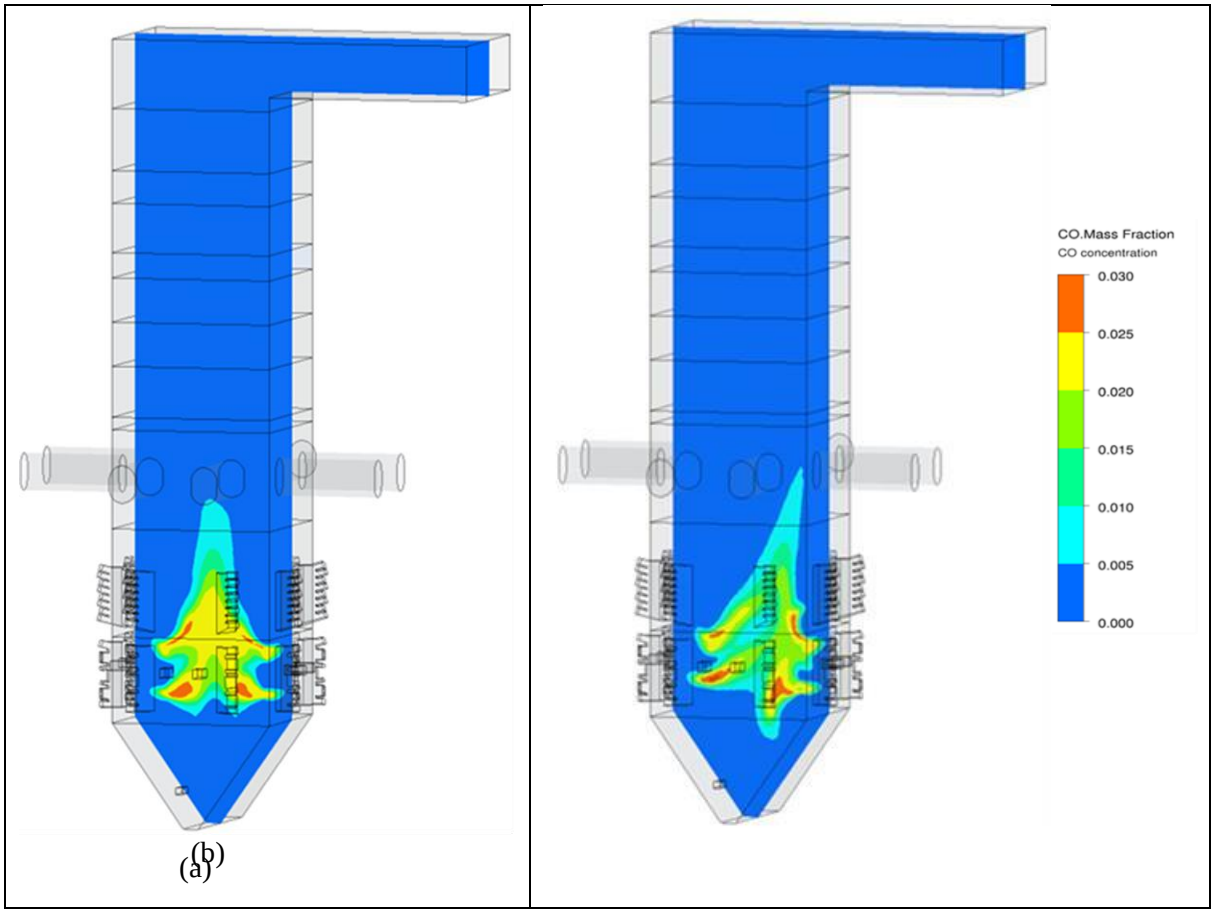

Figure 4. Predicted CO concentration for cases (a) Firing units 2&6 out-of-service (b) Firing units 5&6 out-of-service. CFD model details and boundary conditions can be found in (Tian et al. 2010a; Tian et al. 2010b).

Several approaches can be used to calculate behaviours of gas species specified by the chemistry. The most straight forward one is a species transport approach. In this approach, transport equations for each species (or each species except a constraint species) are solved. To close the transport equations (such as Equation 4), the source term, S_I, needs to be calculated. Usually the gas phase reactions in coal fired boilers can be taken as a fast reaction system in respect to their modelling. A fast reaction system means the chemical reaction rates are much faster than the mixing processes in the system, in other words, reaction rates in the system are controlled by the mixing process. Another characteristic of flames in coal-fired boilers is that they generally can be classified as non-premixed combustion.

The source term S_I can be computed as the sum of the reaction sources of reactions involving species I,

$$S_I = W_I \sum_{k=1}^{N_{KI}} (\nu''_{kI} - \nu'_{kI}) R_{kI}\,, \tag{30}$$

where W_I is the molar mass of species I. R_{kI} is the reaction rate of species I in the reaction k, which can be calculated by using either a finite rate approach or the eddy dissipation model. ν'_{kI} is the stoichiometric coefficient of species I in the reaction k as a reactant and ν''_{kI} is the stoichiometric coefficient of species I in the reaction k as a product. N_{kI} is the number of reactions that component I involves in.

For finite rate chemistry model, the reaction rate of reaction k, R_k, is calculated as:

$$R_k = F_k \prod_{I=A,B,....}^{Nc} [I]^{r'_{kI}} - B_k \prod_{I=A,B,....}^{Nc} [I]^{r''_{kI}} \quad (31)$$

here [I] is the molar concentration of species I. N_c is the number of species in the reaction k. The forward rate constant F_k can be calculated by the Arrhenius rate:

$$F_k = A_k T^{\beta_k} \exp(-\frac{E_k}{RT}) \quad (32)$$

where A_k is the pre-exponential factor; T is temperature; β_k is the temperature exponent; E_k is the activation energy; and R is the universal gas constant, 8.314 J/molK.

If applicable, the backward rate constant B_k can be calculated as:

$$B_k = A_b T^{\beta_{bk}} \exp(-\frac{E_{bk}}{RT}) \quad (33)$$

The finite rate chemistry model is applicable to laminar flames as the effects of turbulence on the reactions are not included. This approach can be used for combustion with relatively slow chemistry and small turbulent fluctuations (Yeoh and Yuen 2009).

In coal-fired flames, the eddy dissipation model (Magnussen and Hjertager 1977) can be used to model the turbulence-chemistry interaction. In the eddy dissipation model for pre-mixed flames, R_k is directly related to the time required to mix reactants at the molecular level, i.e. a mixing time defined by the turbulent kinetic energy of gas mixture, k_g, and dissipation rate, ε_g:

$$R_{kI} = A\frac{\varepsilon_g}{k_g}\min\left(\frac{[I]}{\nu'_{kIR}}\right) \tag{34}$$

where ν'_{kIR} is the stoichiometric coefficient for reactant I in reaction k; and A is a constant with a value of 4.

The advantage of the eddy dissipation model is that it is simple and takes accounts effects of turbulence on chemistry. However, the eddy dissipation model, as shown in Equation 34, does not account for the effects of temperature on reaction rates and it can only be used for one-step or two-step reactions without giving detailed chemistry effects. When more detailed reaction kinetics are required in the CFD model, the generalized eddy dissipation concept model can be used.

In the generalised eddy dissipation concept model, the mean reaction rate of component I, R_I, is assumed to occur in small turbulence structures over a mean residence time τ^* (Magnussen and Hjertager 1981). The fine turbulence structures in a computational cell are characterised a mean length fraction, ξ^*. The mean reaction rate of I, R_I, is calculated as:

$$R_I = \frac{W_I \rho (\xi^*)^2}{\tau^*[1-(\xi^*)^3]}(Y_Y^* - Y_I) \tag{35}$$

Here Y_Y^* is the species mass faction in the fine structures after reacting over the time scale τ^*; Y_Y^* can be determined through a laminar finite rate model (Yeoh and Yuen 2009). The mean residence time τ^* is calculated as:

$$\tau^* = C_\tau \left(\frac{\nu_g}{\varepsilon_g}\right)^{1/2}, \tag{36}$$

here C_τ is a constant with a default value of 0.4082.

The mean length fraction, ξ^* is calculated as:

$$\xi^* = C_\xi \left(\frac{\nu_g \varepsilon_g}{k_g{}^2}\right)^{1/4}, \tag{37}$$

here C_{ξ} is a constant with a default value of 2.1377.

More advanced turbulence-chemical interaction models such as the joint probability density function (PDF) and laminar flamelet models can be applied to coal fired combustion. Nevertheless, these models are computationally expensive. Their advantages over the EDC model and eddy dissipation models have been found to be less pronounced in coal flames than the gas flames, partially due to the fact that gaseous phase reactions are just a part of the reaction sequence involved in coal combustion (Vascellari and Cau 2012): the heterogeneous reaction of char is also important in the coal flame.

3. MODELS FOR PARTICLE PHASE MOTION

In the most CFD studies of PC combustion in furnaces, two categories of approaches are typically used for prediction of the coal particle phase motion: the Eulerian-Eulerian model or the Eulerian-Lagrangian model.

3.1 Eulerian-Eulerian model

The Eulerian-Eulerian model calculates the particle flow using Eulerian or fluid-like equations, e.g. modified Navier-Stokes Equations 1 and 2. These equations can be implemented efficiently in the existing solvers resulting in relatively less computational time being required to calculate mean parameters, such as velocity and volume fraction for the particle flow. Some simplified Eulerian-Eulerian models, which assumed a mechanical and thermal equilibrium between the two phases, have been developed and used to model coal combustion, e.g. Benim et al. (2005), Fiveland and Wessel, (1988). Zhou et al. (2002) developed a two-fluid-trajectory model and simulated coal combustion in a tangentially fired boiler. This two-fluid-trajectory model uses Eulerian gas-phase equations, Eulerian particle-phase continuity and momentum equations, two-phase turbulence models, and Lagrangian ordinary differential equations of particle temperature and mass change to take into consideration of the history effects (Zhou et al. 2002). The Eulerian-Eulerian coal combustion model has been incorporated in the commercial CFD code PHEONICS.

Nevertheless, there are some inherent problems in the use of Eulerian models for gas-particle flows as reviewed by Tian et al. (2005), propably making this approach less attractive in modeling PC combustion.

3.2 Eulerian-Lagrangian model

Most commercial and research CFD codes make use of the Eulerian-Lagrangian approach to model pulverised coal particle combustion, for examples, ANSYS/CFX and FLUENT. The Lagrangian model tracks the individual particle motion and therefore overcomes some difficulties associated with the Eulerian model for the particles (Tian et al. 2005).

The equations of particle motion are:

$$\frac{dx_p}{dt} = u_p \tag{38}$$

$$m_p \frac{du_p}{dt} = F_D + F_g + F_{other}, \tag{39}$$

here F_D is the drag force, F_g is the gravity force and F_{other} includes other forces such as buoyancy force, virtual mass force, pressure gradient force, etc. The drag force F_D is calculated from (Tian et al. 2010a):

$$F_D = m_p \frac{u_{g,instant} - u_p}{\tau_r}, \tag{40}$$

here $u_{g,instant}$ is the instantaneous gas velocity. The discrete random walk (DRW) model is widely used to model the effects of trublence on particle trajectories. In the DRW model, $u_{g,instant} = u_g + u'$ when particle dispersion is taken into consideration (u' is an approximation to the eddy fluctuation velocity determined using a random walk approach); $u_{g,instant} = u_g$ when the particle dispersion is off. The particle relaxation time τ_r is given by:

$$\tau_r = \frac{\rho_p d_p^2}{18 \mu_g f_D} \tag{41}$$

and the drag coefficient f_D for a sphere can be calculated based on empirical equations, e.g. (Tian et al. 2010a):

$$f_D = \begin{cases} 1 + 0.15\mathrm{Re}_p^{0.687}, & \mathrm{Re}_p \le 1000 \\ 0.01833\,\mathrm{Re}_p, & \mathrm{Re}_p > 1000 \end{cases}$$

(42)

$$C_D = \frac{24}{\mathrm{Re}_p} f_D$$

(43)

One major concern of the Eulerian-Lagrangian approach is the expensive computing time that may be experienced when tracking a substantial number of the particles to obtain good statistical information of the particle phase (Tian et al. 2005). With the progress in computer speeds, multi-core processors and parallelisation techniques, the time expense of Eulerian-Largrangian models has been significantly reduced and it has become a popular tool for coal combustion simulations. The Eulerian-Lagrangian model is extended in coal combustion models to take into account the particle combustion processes occurring in the furnace. The most widely used coal drying models, devolatilisation models and char oxidation models that have been implemented the Eulerian-Largrangian models are reviewed in the next section.

3.2.1 Coal devolatilisation and char oxidation models

When pulverised coal particles enter the furnace through the burners, they rapidly mix with hot intermediates and combustion products. The particles undergo the following four well-defined steps during combustion in the furnace (Wu 2005) shown in Figure 5:

- Coal particle heating and drying;
- Devolatilisation of the coal particle to produce non-condensable volatiles (light gases), condensable volatiles (tars), and a carbonaceous char;
- Gas phase volatile combustion;
- Char combustion.

3.

Volatile Combustion

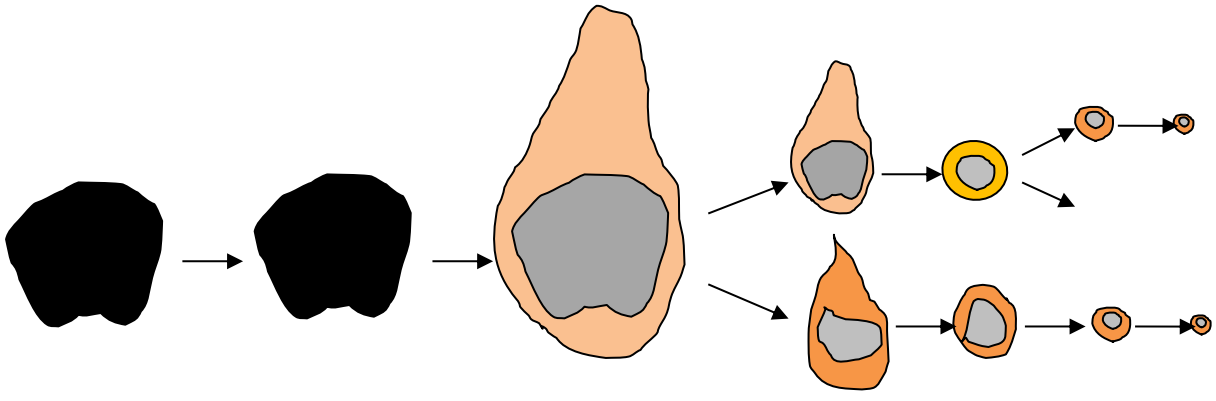

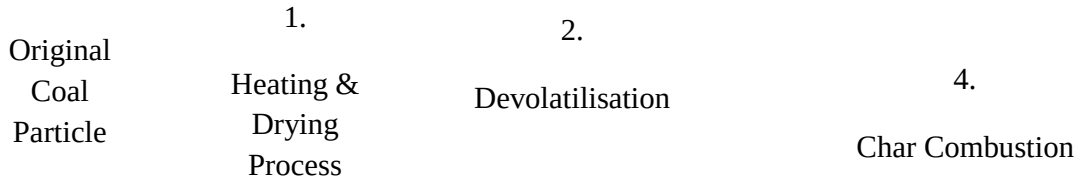

Figure 5. Coal particle combustion processes, after (Wu 2005).

To model these processes in the Lagrangian particle tracking model, the coal particles are normally treated as spheres that do not interact with other particles. Each particle is able to undergo internal reactions as well as being fully coupled through the transfer of mass, momentum and energy with the gas phase, which enables heat transfer and chemical reactions to occur between the particle and gas phase. Several models are required to model the combustion of the coal particles shown in Figure 5, namely, the drying model for the raw coal particles, a devolatilisation model, and a char combustion model.

Coal normally contains moisture that can be divided into surface moisture and inherent (or bound) moisture. Surface moisture is moisture on the coal surface including inter particle voids and contact points of particles; while inherent moisture exists in the coal internal pore structure (Wu 2005). Old coal such as bituminous coals has 1-12.2% moisture as received and subbituminous coals have moisture as received in the range of 14.1-31% (Tillman 1991; Wu 2005). Young coals such as brown coal and lignite normally contain higher moisture content, e.g. Victorian brown coal typically has 66-70% moisture by weight (Tian et al. 2010b). In pulverised coal furnaces, a fraction of water in coal particles is released from coal during the pulverising process and also in the pre-drying process if there is any. The content of the water in particles entering the furnace depends on the coal type and the boiler type.

Sometimes the modelled drying process of coal particles in PC furnaces can be incorporated in the devolatilisation process, or it can be modelled in a separate drying model. When the water content of the particles is small, e.g. coal particles after a pre-drying process, evaporation of water in the pre-dried particle can be modelled as a species of volatile gas. This will slightly reduce the complexity of the coal modelling process by eliminating the need for a separate drying model. However, it is more accurate to model the evaporation of water separately from the devolatilisation process, because in real furnace combustion, most water in the particles evaporates before the start of devolatilisation process.

Typical equations used to model the water evaporation in coal particles assuming mass transfer control are given in Bhambare et al. (2010). The change of mass of coal particles during the drying process can then be calculated as below:

$$(\frac{dm_p}{dt})_{drying} = k_c(C_{vapour,s} - C_{vapour,\infty})A_p M_{vapour}\ , \tag{44}$$

here A_p is particle surface area. M_{vapour} is the molar mass of water vapour. k_c is mass transfer coefficient. $C_{vapour,s}$ is vapour concentration at the coal particle surface:

$$C_{vapour,s} = \frac{p_{sat}(\mathrm{T}_P)}{\mathrm{R}T_p}, \tag{45}$$

here $p_{sat}(\mathrm{T}_P)$ is the saturated vapour pressure at the particle temperature, T_p. $C_{vapour,\infty}$ in Equation 44 is the vapour concentration in the bulk gas:

$$C_{vapour,\infty} = [\mathrm{H_2O}]\frac{p_{op}}{\mathrm{R}T_\infty}\ , \tag{46}$$

here, $[H_2O]$ is the mole fraction of H_2O vapour and p_{op} is the operating pressure.

The mass transfer coefficient, k_c, in Equation 44 is calculated using the Nusselt number:

$$Nu = \frac{k_c \mathrm{d}_P}{D_{vapour,m}} = 2.0 + 0.6Re_d^{1/2}Sc^{1/3} \tag{47}$$

where $D_{vapour,m}$ is the diffusion coefficient of vapour, S_c is the Schmidt number.

In the CFD model, the reduction of particle mass can be accounted for either by reducing the particle density without changing of the particle diameter or reducing the particle diameter with a constant density.

3.2.2 Devolatilisation models

After drying in the burner exit region, coal particles are heated to higher temperatures rapidly, and start to decompose to produce volatiles and tars. Volatiles are non-condensable gases that consist mainly of a mixture of CO_2, H_2O vapour and combustible gases including CO, H_2 and hydrocarbons such as CH_4, C_2H_4, C_2H_6, etc. (Field et al. 1967). The tar is a heavy hydrocarbon-like substance that is condensable, with an atomic ratio of H/C >1.0 (Tillman 1991; Wu 2005). Again, the exact products of the devolatilisation process are determined by the coal types and decomposition condition that can be either rapid or slow. Pulverised coal combustion always involves a high rate of heating (10^4 K/s or greater) that is classified as rapid decomposition (Field et al. 1967). Evolution of volatile matter under the influence of heat and the subsequent

combustion of the vapours evolved is an integral part of the combustion of coal, including brown coal (Mulcahy et al. 1991). In fact, about 65% of the heat released by combustion of Yallourn coal, one kind of Latrobe Valley coal, is derived from combustion of the volatiles (Jones and Stacy 1986).

Two groups of devolatilisation models have been developed and used for PC combuston models: simple global kinetic models and more comprehensive computer-based network models. In CFD models, the products of devolatilisation process are assumed to be the gas(es) and that remaining coal particles that comprise char and ash only. Volatile gas(es) in the model can be a single species or several major volatile components such as CH_4, C_2H_4, C_2H_6, etc. Two simple global kinetic models are widely used in PC coal combustion modelling. These are the single first-order reaction (SFOR) model and the competing reaction model.

In SFOR model the devolatilisation of coal particles is assumed to be independent of the particle size, porosity, specific surface area and surface/mass ratio, and other coal characteristics (Tillman 1991). The rate of devolatilisation is assumed to be first-order dependent on the amount of volatiles remaining in the particle:

$$(\frac{dm_p}{dt})_{devo} = -k_v[m_p - (1- f_{v,0})m_{p,0}] \quad (48)$$

where m_p is the instantaneous particle mass, $m_{p,0}$ is the initial particle mass after drying process if there is a separate drying model. $f_{v,0}$ is the initial mass fraction of volatiles in the particle before devolotiliation and k_v is the kinetic rate:

$$k_v = A_v \exp(-\frac{T_v}{T_p}) \quad (49)$$

The pre-exponential factor A_v and the activation temperature T_v are constants determined experimentally for the particular coal.

Some experiments have found that the yield of volatiles from PC particles can be greater by as much as a factor of two than the proximate value in PC furnaces (ANSYS/CFX 2015). The competing reaction model takes this into consideration by assuming that two devolatilisation process undergo simultaneously, one reaction dominants at low temperatures and the other at high temperatures (ANSYS/CFX 2015). Therefore, Equation 48 can be written as:

$$(\frac{dm_p}{dt})_{devo} = -(k_{v,1}\alpha_1 + k_{v,2}\alpha_2)[m_p - (1 - f_{v,0})m_{p,0}], \quad (50)$$

where α_1 is near the proximate volatile fraction where α_2 is higher, close to unity, reflecting the characteristics of devolatilisation at high temperature (Wu 2005). $k_{v,1}$ and $k_{v,2}$ are the kinetic rate at low and high temperature, respectively.

A chemical percolation model for devolatilisation (CPD) model has been developed in Grant et al.(1989) by applying the lattice statistics. In contrast to the above devolatilisation models based on empirical rate relations, the CPD model characterises the devolatilisation behaviour of rapidly heated coal based on the physical and chemical transformations of the coal structure (ANSYS/FLUENT 2015). The CPD has been implemented into several CFD codes such as ANSYS/FLUENT and has been used for some coal combustion modelling, e.g.in Jovanovic et al.(2012). In this chapter, the CPD model is not discussed in details due to the space limitation. Interested readers can read more details in Grant et al.(1989) and Wu (2005) .

Devolatilisation of Latrobe Valley brown coal under fast heating rates (normally larger than 10^4 K/s), which is experienced in pulverised brown coal combustion, has been investigated in several studies using different methods such as a vertical laminar-flow furnace (Roberts and Loveridge 1969), a plug-flow reactor (Duong 1985), and a pressurised drop-tube furnace (Yeasmin et al. 1999), and corresponding kinetic parameters for the SFOR model have been calculated based on the experimental measurements. Duong (1987) conducted measurements of pulverised brown coal combustion in a plug-flow reactor under different inlet conditions. It is found that the fuel/air mass ratio is seen to be the only factor affecting both the rates and mechanism of the volatile release. However, this cannot explain the large difference between parameters developed in Roberts and Loveridge (1969) and Yeasmin et al. (1999), given that both experiments were carried out in an inert atmosphere of nitrogen. The kinetics parameters from Yeasmin et al. (1999) and Duong (1987) have been tested in a drop tube furnace (Ouyang et al. 1998) and it was found the parameters from run 3 and run 5 of Duong (1987) give better agreement than other parameters for the measured particle mass loss along the axis line in the drop tube furnace.

It has been found that some bituminous coals swell considerably during heating. A swelling coefficient can be used in CFD codes to take into account such swelling effects during devolatilisation. The value of the swelling coefficient is determined by coal types and

combustion conditions. Experiments have shown that Latrobe Valley coals do not undergo swelling but develop an internal bubble structure when devolatilised in nitrogen (Sainsbury and Hawksley 1969). The non-swelling characteristic is confirmed by the observations of several combustion experiments such as in Street (1979). Therefore, the particle swelling can be neglected when simulating the Latrobe Valley coal combustion using CFD.

3.2.3 Char combustion models

Char remaining in the coal particle after devolatilisation contains fixed carbon and subsequently undergoes a heterogeneous reaction with gaseous species at elevated temperatures (Wu 2005). Combustion of the residual char is relatively slow due to the small reaction surface. The heterogeneous reactions in a coal particle include five steps shown in Figure 6 (Williams et al. 2000; Wu 2005):

Step 1. Diffusion of oxidants through the gas boundary layer surrounding the particle (external diffusion) and through the pores of the particle (internal diffusion) to the particle surface

Step 2 adsorption of reactants onto the particle surface

Step 3 surface reactions to form solid products

Step 4 desorption of the solid products into the gas phase

Step 5 diffusion of gas phase oxidisation products through the pores of the particle and through the ambient gas phase to the gas stream (Williams et al. 2000; Wu 2005).

In pulverised coal combustion, the main heterogeneous reactions include:

$$C + O_2 \rightarrow CO_2 \tag{51}$$

$$C + \frac{1}{2} O_2 \rightarrow CO \tag{52}$$

Reaction 51 dominates at lower temperature and reaction 52 is dominant with increasing temperature. Furthermore, residual char may also react as follows:

$$C + CO_2 \rightarrow 2CO \tag{53}$$

$$C + H_2O \rightarrow CO + H_2 \quad (54)$$

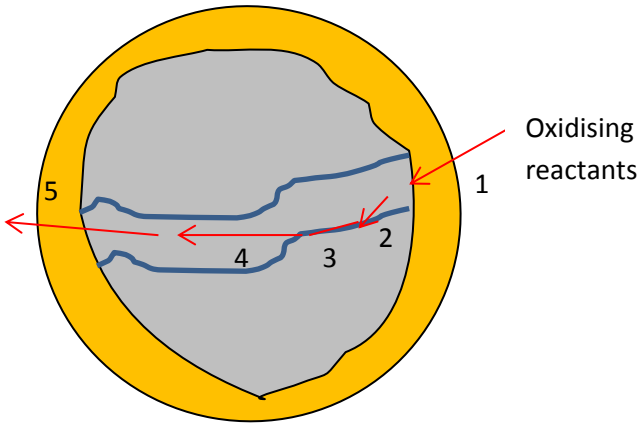

Figure 6 Steps in heterogeneous reactions, after Williams et al. (2000).

CO and H_2 produced in the above heterogeneous reactions diffuse away from the char particle into the ambient gas stream and react as follows:

$$CO + \tfrac{1}{2} O_2 \rightarrow CO_2 \quad (55)$$

$$H_2 + \tfrac{1}{2} O_2 \rightarrow H_2O \quad (56)$$

$$CO + H_2O \rightarrow CO_2 + H_2 \quad (57)$$

Combustion of a char particle is controlled by the rate of oxygen diffusion to the particle or the chemical reaction rate, or a combination of the two factors (Wu 2005). In the low temperature zone (<600°C), the chemical reaction is relatively slow and the available oxygen at the particle surface can readily diffuse into the pores of the particle and react with carbon (Tillman 1991). The char oxidation is determined by the chemical reaction rate rather than the rate of oxygen diffusion. In the moderate temperature zone (about 600-800°C), the chemical reaction rates become higher and consume oxygen faster. Both the chemical reaction and oxygen diffusion determine the char oxidation rate (Wu 2005). When the temperature increases further, the chemical reaction becomes so fast that the oxygen diffusion cannot follow. The oxygen concentration at the particle external surface diminishes to zero and no oxygen is left to diffuse into the pores (Wu 2005). Therefore, char oxidisation rates are determined by the oxygen diffusion rate to the particle surface and diffusion rate of oxygen through the porous ash layer to the active char layer.

Several char oxidation models have been developed, mainly depending on the reaction mechanism for the combustion. Some of these models are global reaction models such as the diffusion-limited surface reaction model, the kinetic/diffusion surface reaction rate model, and other models such as the Gibb model. The kinetic/diffusion reaction rate model, both diffusion of oxidising reactors and surface reaction rate control the total reaction rate of the char. The kinetic/diffusion surface reaction rate model is given as follows:

$$(\frac{dm_p}{dt})_{char} = -\pi d_p^2 \rho_g R_T [O_2] \frac{P_g}{P_A} \quad (58)$$

where R_T is overall reaction rate:

$$R_T = (R_{diff}^{-1} + R_C^{-1})^{-1} \quad (59)$$

R_{diff} is the diffusion rate coefficient:

$$R_{diff} = \frac{D_{ref}}{d_p} \left(\frac{T_p + T_g}{2T_{ref}} \right)^{\alpha} \frac{P_A}{P_g} \quad (60)$$

where D_{ref} is the dynamic diffusivity; T_{ref} is the reference temperature normally 293K.

R_c is the chemical rate coefficient:

$$R_C = A_C \exp(-\frac{T_C}{T_P}) \quad (61)$$

where A_c and T_c are determined by the type of coal and specified as input parameters.

For the diffusion-limited model, R_c is considered large enough, so based on Equation 59, R_T is controlled by R_{diff} that is the diffusion process of oxidant to the reaction surface. Therefore, $R_T=R_{diff}$.

In the Gibb's model (Gibb 1985) as cited in (ANSYS/CFX 2015), the oxidation mechanism of carbon can be characterised by the parameter ϕ:

$$\phi C + O_2 \rightarrow 2(\phi - 1)CO + (2 - \phi)CO_2 \quad (62)$$

Here ϕ is the molar ratio of carbon atom to oxygen molecules, determined by the particle temperature:

$$\frac{2(\phi-1)}{2-\phi} = A_s \exp(-\frac{T_s}{T_p}) \quad (63)$$

A_s has a value of 2500 and T_s is 6240 K (ANSYS/CFX 2015). After solving the above analytic equation, the rate of particle mass loss is calculated:

$$(\frac{dm_p}{dt})_{char} = -\frac{3\phi}{1-\varepsilon_c}\frac{M_c}{M_{O_2}}\frac{\rho_\infty}{\rho_c}(k_1^{-1}+(k_2+k_3)^{-1})^{-1}m_p \quad (64)$$

where ε_c is char particle void faction; k_1 is the rate of external diffusion:

$$k_1 = \frac{D}{r_p^2} \quad (65)$$

Here D is the oxygen diffusion coefficient in the ambient gas. k_2 is the surface reaction rate:

$$k_2 = (1-\varepsilon_c)\frac{k_c}{R} \quad (66)$$

k_c is the carbon oxidation rate:

$$k_c = A_c T_p \exp(-\frac{T_c}{T_p}) \quad (67)$$

A_c is 14 m/sK and T_c is 21580 K (ANSYS/CFX 2015). k_3 in Equation 64 is the rate of internal diffusion and internal surface reaction:

$$k_3 = k_c(\beta_c \coth\beta_c - 1)/(\beta_c^{\,2} a_C) \quad (68)$$

where $\beta_c = R(\frac{k_c}{D_p \varepsilon_c a_C})^{0.5}$; a_c is 0.75. D_p is computed from external diffusivity D, according to $D_p = effic \times D$.

There are other surface reaction rate models such as intrinsic model. However, these models are not given due to the space limit. Interested readers are referred to publications by Edge et al. (2011) and Mitchell (2000) for further details.

3.3 Radiation models

In pulverised coal boilers, thermal radiation is the dominant mode of heat transfer. In a combustor, radiant heat transfer from the flame and combustion products to the surrounding walls can be predicted if the radiative properties and temperature distributions in the medium and on the walls are available (Viskanta and Mengüç 1987). In CFD models of pulverised coal

furnaces, a radiative transfer equation (RTE) is normally employed to model radiation in the furnace (Tian et al. 2010a):

$$\frac{dI_{\upsilon}(\vec{r},\vec{s})}{ds} = -(K_{a\upsilon} + K_{s\upsilon})I_{\upsilon}(\vec{r},\vec{s}) + K_{a\upsilon}I_b(\upsilon,T_g) + \frac{K_{s\upsilon}}{4\pi}\int_0^{4\pi} dI_{\upsilon}(\vec{r},\vec{s})\Phi(\vec{s}\cdot\vec{s}')d\Omega' \qquad (69)$$

Here, I_v is the spectral radiant intensity that depends on position $\vec{r}$ and direction $\vec{s}$. $\vec{r},\vec{s},\vec{s}'$ are position vector, direction vector, and scattering direction vector, respectively. $K_{a\upsilon}$ is the spectral absorption coefficient and $K_{s\upsilon}$ is the spectral scattering coefficient. I_b is blackbody emission intensity; Ω' is the solid angle.

The RTE is very difficult to solve directly due to the differential and integral processes in the equation. Therefore, several radiation models have been developed such as Monte Carlo model, discrete transfer (DT) model and P-1 model; these have been used in modelling coal flames in pulverised coal furnaces.

The Monte Carlo model simulates the rays of radiation as photon trajectories and has been recognised as the best method for modelling radiation (IIBD 2002). However for coal-fired boilers, the computational time is extensive, making this model less attractive.

For DT model, the scattering in the furnace is assumed to be isotropic and the system is assumed to be reasonably homogeneous; the intensity I_v along rays leaving from the boundaries is solved using the equation of transfer (ANSYS/CFX, 2009}:

$$I_v(r,s) = I_{v0}\exp(-(K_{av}+K_{sv})s) + I_{bv}(1-\exp(-K_a s)) + K_{sv}\bar{I}_v \qquad (70)$$

where I_{v0} is the radiation intensity leaving the boundary. The radiation intensity is then integrated over a defined solid angle at discrete points to get the spectral incident radiation, and the radiative heat flux; based on the homogeneity assumption the solution is extended to the entire domain (ANSYS/CFX 2015).

In the P-1 model I_v is represented by an orthogonal series of spherical harmonics (Sazhin et al. 1996). In the PC furnace, P-1 model assumes that radiation intensity is isotropic anywhere in the CFD domain. In the P-1 model the following equation is solved:

$$-\nabla\left(\frac{1}{3(K_{av}-K_{sv})-AK_{sv}}\nabla G_v\right) = K_{av}(E_{bv}-G_v) \qquad (71)$$

here G_v is spectral incident radiation

$$G_v = \int I_v d\Omega_s \tag{72}$$

and A is the linear anisotropy coefficient. The thermal heat transfer is linked to the energy equation by the term $-\nabla q_{rv}$ (Sazhin et al. 1996):

$$\nabla q_{rv} = -\nabla \frac{1}{3(K_{av} - K_{sv}) - AK_{sv}} \nabla G_v \tag{73}$$

The P-1 model is one of a number of flux methods that separate the dependency of radiation intensity from the spatial dependency by discretization of the intensity into vectors representing intervals of the solid angle. P-1 model has been proved adequate for the study of pulverised fuel flames in regions away from the immediate vicinity of the flame. This is because P-1 model is particularly useful for accounting for the radiative exchange between gas and particles (Sazhin et al. 1996). The predicted wall incident heat flux for a brown coal furnace based on DT and P-1 radiation model are compared against power plant measurement and it is found that P-1 model under-predicts the incident heat flux considerably (Tian et al. 2010a). This demonstrates that these radiation models are not universal but case sensitive.

Another important aspect in radiation is spectral modelling. Several models can be used for spectral integration in CFD modelling of radiative heat transfer, e.g. gray model, multiband model and weighted sum of gray gases model (WSGGM). For gray model, the furnace gas properties are assumed not to be a function of wavelength, therefore saving computing time for integration of radiation intensity over spectrum. However, this simple approach is not accurate for coal flames as gases in the coal-fired furnaces such as CO_2 and water vapour have significant different spectral properties. In multiband models, gas properties and radiation sources are represented by a stepwise function. The radiative flux can be calculated by the integration through the stepwise function. In coal combustion CFD practice, the WSGG model is also widely used. In WSGG, the emissivity and absorptivity are approximated by the summation of gray media solutions, normally CO_2, water vapour and hydrocarbon fuels.

3.4 Emissions modeling

Emissions from the tangentially fired boilers have been intensively studied using CFD techniques. The major emission of concern is NO_x, e.g. Backreedy et al. (2005), Díez et al. (Díez et al. 2008), and Le Bris et al. (Le Bris et al. 2007), because of the established restrictive legislations that limit NO_x emissions to the atmosphere (Díez et al. 2008).

The level of NO_x emissions is dependent on the nitrogen content in the coal and the combustion conditions (Hodges and Holden 2003). Nitrogen levels in Latrobe Valley brown coals are very low by world standard and the separation firing system of the Latrobe Valley boilers achieves a staged combustion by introducing about 20% of the fuel above the main burners, resulting in comparatively low NO_x emission.

In CFD models, the concentration of nitric oxide (NO) is normally modelled because NO is the major NO species in emissions from pulverised coal power plant (Visona and Stanmore 1998). As the concentration of NO is low in pulverised coal furnaces, its effects on combustion in the furnace is negligible, so it can be modelled after the flow fields, temperature fields and major species field are solved. Nitrogen chemistry is extremely complex and modelling of details of chemical reactions of NO is very difficult, therefore simple global reactions are usually used to model NO formation and destruction in CFD models (Jones et al. 1998).

The major formation mechanisms of NO emissions in PC power plant are known as thermal NO, prompt NO and fuel NO. The formation of thermal NO is dependent on the temperature of the PC furnace. When the temperature in PC furnace is high (typically greater than 1500˚C), free radicals such as O and N from atmospheric oxygen and nitrogen are abundant and start forming NO (Li et al. 2004). Major reactions forming thermal NO are given as below (Li et al. 2004):

$$N_2 + O \underset{k_{-N1}}{\overset{k_{N1}}{\leftrightarrow}} NO + N \tag{74}$$

$$N + O_2 \underset{k_{-N2}}{\overset{k_{N2}}{\leftrightarrow}} NO + O \tag{75}$$

$$N + OH \underset{k_{-N3}}{\overset{k_{N3}}{\leftrightarrow}} NO + H \tag{76}$$

The Arrhenius form can be used to calculate reaction rate, k_{Ni} or k_{-Ni} for each reaction. The rate of thermal NO formation is therefore calculated by the following equation (Li et al. 2004), under the assumption of quasi steady state:

$$\frac{d[NO]_t}{dt} = 2k_{N1}[N_2][O_2]\frac{1-[NO]^2/k_N[N_2][O_2]}{1+k_{-N1}[NO]/(k_{N2}[O]+k_{N3}[OH])} \tag{77}$$

Here k_{N1}, k_{N2}, k_{N3} are reaction rates of reaction (74-76), respectively. $k_N = (k_{N1}/k_{-N1})(k_{N2}/k_{-N2})$.

The complete mechanisms for prompt NO formation are complex and usually prompt NO is higher in rich flames than in lean flames. A single global model is usually used to calculate prompt NO formation as below (Li et al. 2004):

$$\frac{d[NO]_{prompt}}{dt} = f_N T^{\beta_{NO}} A_{pr} [O_2]^{\alpha_{NO}} [N_2][Fuel]^{b_{NO}} \exp(E_a / RT_g) \quad (78)$$

where f_N is a correction factor. A_{pr} is the pre-exponential factor; a_{NO} and b_{NO} are reaction orders.

Fuel NO accounts for 70-90% of NO emission in fossil fuel combustion and is the major part of NO emissions in fossil fuel combustion (Li et al. 2004). Fuel NO is mainly formed from the nitrogen compounds in the coal and HCN has been found to be the major precursor of fuel NO. Major reactions for formation of fuel NO in many CFD models are as below:

$$HCN + O_2 \underset{k_{-N4}}{\overset{k_{N4}}{\leftrightarrow}} HCO + NO \quad (79)$$

Again an Arrhenius form of reaction rates can be used to calculate k_{N4} and k_{-N4} of the above reactions. When reactions 76 and 79 are included in the CFD coal model, the species transport equations of HCN, HCO and OH will be included as well.

Another concern of emissions is the emission of SO_x that contributes to acid rain and the corrosion of power plant equipment. More than 50% of SO_x emission in the world is from coal fired power plants (Perera and Faltsi-Saravelou 2007). Coals have sulphur concentration that varies from 0.2 % to 11% by weight depending on coal type and the environmental conditions (Boardman and Smoot 1993; Wu 2005). Sulphur exists in coals in two different forms, pyritic and organic sulphur and after combustion, most sulphur converts to SO_2 (about 90%) and a small fraction of sulphur is captured in the ash (Wu 2005). The mechanisms of sulphur oxidation are complex and can be modelled by either by a global model or reduced mechanism (Perera and Faltsi-Saravelou 2007).

The levels of sulphur in Latrobe Valley coals are very low by world standards (typically 0.2% dry-based) and a significant portion (10~30%) of the sulphur is retained in the ash by sulphation of basic inorganic oxides (Kiss et al. 1984). Therefore, the sulphur emission from Latrobe Valley power stations are below licence limits without the need for flue-gas desulphurisation (Hodges and Holden 2003).

Soot is also an emission problem from PC power plants. Furthermore, soot plays an important role in radiative heat transfer in the furnace. Therefore a soot model is required to accurately calculate heat transfer and understand emission problems from PC furnaces. Many methods have been developed to model soot formation in gaseous flames. However these methods may not be appropriate to use in coal flames, as tar is the principle precursor to soot in a coal flame, while acetylene is the major precursor to soot in gaseous hydrocarbon flames (Brown and Fletcher 1998). Therefore, it is critical to include a tar transport equation in the CFD coal soot model.

Several coal soot models have been developed in the literature and one advanced model is from Brown and Fletcher (1998). In this model, the equations of mass fraction of soot (Y_c) and tar (Y_T) are given as below (Brown and Fletcher 1998):

$$\nabla \cdot \left(\rho_g U_g Y_C\right) = \nabla \cdot \left(\frac{\mu}{\sigma} \nabla Y_C\right) + S_C \tag{80}$$

$$\nabla \cdot \left(\rho_g U_g Y_T\right) = \nabla \cdot \left(\frac{\mu}{\sigma} \nabla Y_T\right) + S_T \tag{81}$$

A transport equation of soot number (Nc) is also included (Brown and Fletcher 1998):

$$\nabla \cdot \left(\rho_g U_g N_C\right) = \nabla \cdot \left(\frac{\mu}{\sigma} \nabla N_C\right) + S_N \tag{82}$$

Source terms of the above equations are (Brown and Fletcher 1998):

$$S_{Y_C} = \rho_g (\dot{r}_{FC} - \dot{r}_{OC}) \tag{83}$$

$$S_{Y_T} = \rho_g (\dot{r}_{FT} - \dot{r}_{FC} - \dot{r}_{GT} - \dot{r}_{OT}) \tag{84}$$

$$S_{N_C} = \rho_g ((N_a / M_C C \min) - \dot{r}_{AN}) \tag{85}$$

where

$$\dot{r}_{FT} = SP_{tar} \tag{86}$$

$$\dot{r}_{OT} = \rho_g [c_T][c_{O_2}] A_{OT} e^{-E_{OT}/RT} \tag{87}$$

$$\dot{r}_{GT} = [c_T] A_{GT} e^{-E_{GT}/RT} \tag{88}$$

$$\dot{r}_{FC} = [c_T] A_{FC} e^{-E_{FC}/RT} \tag{89}$$

$$\dot{r}_{OC} = SA_{v.C} \frac{P_{O_2}}{T^{1/2}} A_{OC} e^{-E_{OC}/RT} \tag{90}$$

$$SA_{v.C} = (6^{2/3} \pi^{1/3} (\rho_g N_C)^{1/3} Y_C^{2/3} \rho_g^{2/3}) / \rho_C^{2/3} \tag{91}$$

$$\dot{r}_{AN} = 2C_a (\frac{6M_C}{\pi \rho_C})^{1/6} (\frac{6kT}{\rho_C})^{1/2} (\frac{\rho_g Y_C}{M_C})^{1/6} (\rho_g N_C)^{11/6} \tag{92}$$

The Arrhenius constants in the above equations can be found in the literature, for example (Brown and Fletcher 1998).

The model has been validated against limited data available in a flat flame and reasonable agreement was achieved (Brown and Fletcher 1998). However, more detailed and reliable measurements of soot and tar in coal flames are not yet available and are required to further develop, tune and validate this model. Furthermore, the effect of turbulence on the soot transport and formation is not clear in the model.

Ash particle dispersion, fouling and slagging present another issue where CFD modelling can provide benefits. Slagging is the deposition of particles (ash, coal) on the furnace parts where radiative heat transfer is dominant, e.g. the water wall tubes and superheater tubes. Fouling is the deposition of ash on the convective parts of the boiler. The ash yields of Latrobe Valley coals are lower than other overseas low rank coals and generally between 1~3% dry-based (Hodges and Holden 2003). However, fouling and slagging remains a major concern for boiler operators. Figure 7 shows a picture of the slagging in the superheater of the tangentially fired brown coal boiler in a brown coal power station in the Latrobe Valley.

Figure 7. Slagging on the superheater tubes in a brown coal power station boilers.

Table 1 shows the predicted flue gas exit temperature (FGET) of the unit No. 3 at TRUenergy's Yallourn power plant without considering slagging and when a slagging layer thickness of 25 mm is accounted for. It can be seen that the FGET increases when the slagging layer thickness increases. For moderate fouling brown coals such as Yallourn and Loy Yang brown coal, the designed FGET is about 1050 C°. The FGET is much higher than 1050 C° when there is a slag layer of 25 mm (about 130 C° higher). The increase of FGET is quite likely to have a negative effect on the fouling behaviour of ash downstream the convective parts of the furnace.

Slagging Layer Thickness (mm)	Flue gas exit temperature (C°)
0	1091
25	1181

Table 1. Predicted flue gas exit temperature for cases with clean condition (no slagging layer) and with slagging layer thickness =25 mm.

Figure 8 shows the predicted gas temperature at the mid-plane of the furnace with and without a slagging layer. The temperature of the case with 25 mm slagging layer (b) is higher than the clean condition case (a) in the center zone of furnace at the primary burner level. The high temperature zone is further increased when the slagging layer thickness is further increased. This increased temperature is due to the reduction of heat transfer to the water walls by the presence of the slagging layer. The increased temperature in the center zone of the furnace leads to the increased FGET.

Figure 8. Predicted gas temperature at the mid-plane of the furnace for cases, (a) clean condition (no slagging layer), (b) slagging layer thickness =25 mm.

The above calculations given in Table 1 and Figure 8 are based on the boundary condition that

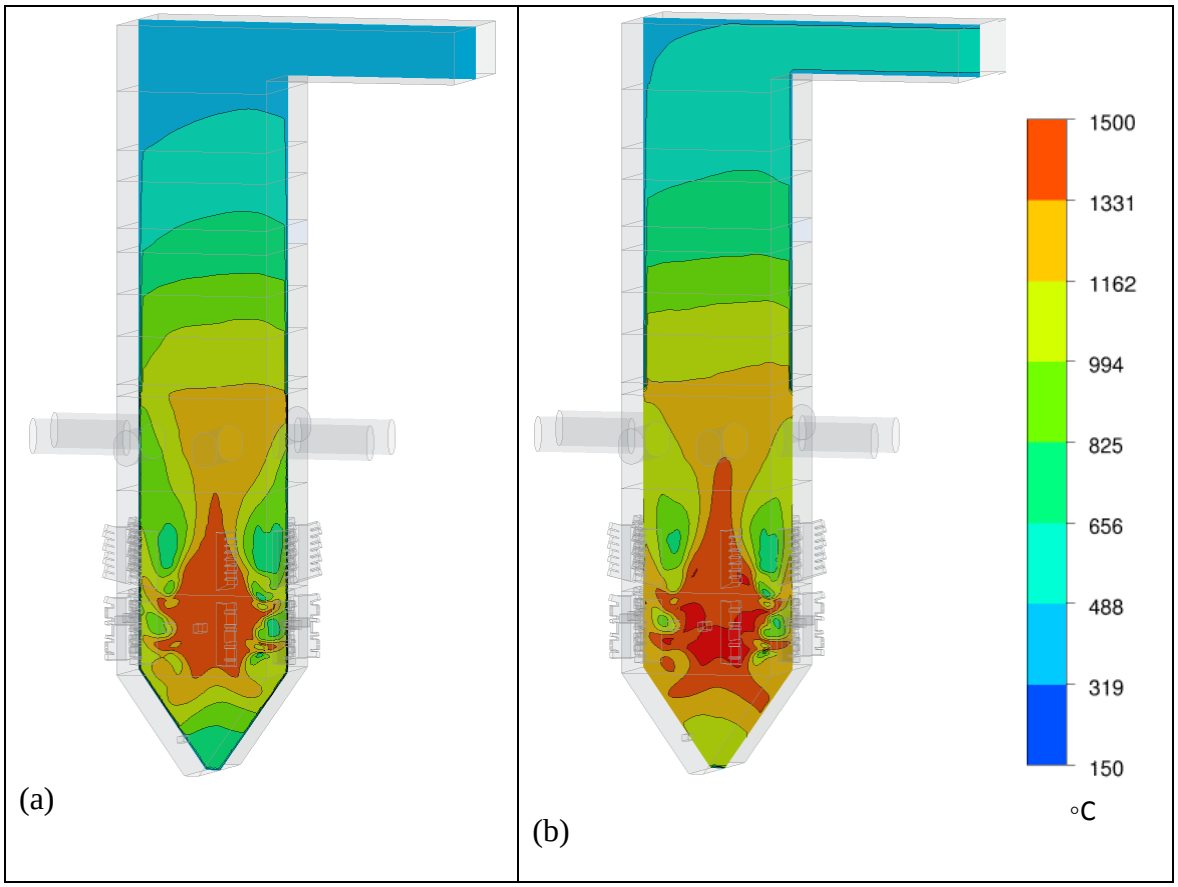

assumes the thickness of slagging layer in the furnace to be uniform. When the exact distribution of slagging layer thickness is required, a slagging model is necessary to calculate the distribution of the slagging layer thickness and to provide more accurate boundary conditions to the gas phase predictions.

Several slagging models have been developed for CFD modelling of coal gasification. Seggiani (1998) developed a one dimensional slag model that is coupled with a 3 dimensional (3D) CFD coal gasifier code. The 3D CFD code provides the particle deposition mass flow rate, particle temperature, and gas temperature to the slag model. The slag model calculates the slag mass flow rate, liquid slag layer thickness, solid slag layer thickness, slag layer outside surface temperature, refractory temperature, etc., based on the slag mass conservation equation, energy conservation equation for the refractory wall and momentum conservation equation (Seggiani 1998). The slag layer outside surface temperature is sent back to the 3D CFD code as the wall boundary condition. This slag model is 1D since it only calculates the slag distribution in an

axial direction. Wang et al. (2007) included a wall burning model into the 1D slag model. The wall burning model is able to calculate combustion of particles captured by the slagging layer.

Recently, Chen et al. (2013) developed a 3D slag model for coal combustion and gasification. In this model, a volume-of-fluid (VOF) model is used to calculate the slag phase which interacts with a Langrangian particle tracking model. This model is able to calculate slag distributions and flows in a 3D manner. Nevertheless, the 3D slag model is still not able to predict the solid slag and further work is needed to capture the solid slag (Chen et al. 2013)

4. CONCLUSIONS

In 2010, coal-fired electricity generation accounted for 40% of the electricity generation worldwide. These plants rely on pulverised coal combustion carried out in large furnaces with multiple interacting burners. Flow and thermal conditions in the furnaces are not easily understood because they involve complex turbulent flow fields interacting with complicated combustion processes and heat transfer. In real industrial installations, additional complications arise from slagging and fouling of heat transfer surfaces, variability in feed characteristics and inevitable uncertainties in actual structural geometry due, for example, to occasional damage or maintenance issues. Design and improvement of these furnaces can be effectively assisted by using numerical modeling with CFD techniques to develop a detailed picture of the conditions within the furnace, and the effect of operating conditions, coal type, and furnace design on those conditions.

The equations governing CFD models of pulverised coal combustion are described, with a focus on sub-models needed for devolatilisation, combustion and heat transfer. The use of the models is discussed with reference to examples of CFD modelling of brown coal fired furnaces in the Latrobe Valley in Australia and black coal fired furnaces described in the literature. Extensions of the CFD models that are required to tackle specific industrial and environmental issues are also described. These issues include control of NO_x, SO_x, and soot emissions and the effect of slagging and fouling on furnace and boiler operation.

In a PC furnace, fine coal particles pulverised in mills are blown into the furnace through burners. Once the particles enter the furnace, they are heated by the hot furnace gas and radiation from the flame, causing drying and devolatilisation. Combustion of the volatiles occurs, followed by char combustion. The furnace gases (together with remaining ash) flow through to the convective heat transfer sections.

As a result, a CFD model of the process must include, in addition to the basic gas flow, sub-models to account for the complex physics and chemistry involved. These include: (1) particle phase model for particle phase motion, (2) evaporation/drying model, (3) devolatilisation model, (4) char combustion model, (5) turbulence model, (6) turbulence-reaction interaction model (gas phase reaction models), (7) radiation model, (8) soot model, (9) NOx model, (10) SOx model, (11) slagging model. (Tian et al., 2010a).

Because of the crucial importance of mixing on combustion and heat transfer, the turbulence model is critical for achieving a reliable basis for a furnace model. Both the standard k-ε model and the SST model appear to perform satisfactorily, although various enhancements have been found to improve the prediction of specific aspects of the flow. In the case of swirl burners, higher order turbulence models such as the RSM are required.

As with turbulence, the sub-model for radiative transfer is of great importance in generating a reliable basis for the over-all model, because so many of the sub-processes involved in coal combustion are temperature dependent. The Monte Carlo method is the best technique for modelling radiation, but is computationally very expensive. The Discrete Transfer (DT) method and the P-1 flux method have been found to be adequate in most PC furnace cases.

Coal devolatilisation and combustion are modelled by means of equations that depend on local gas and particle temperatures, and local concentrations, as predicted by the CFD model. Various sets of equations have been developed, with the complexity of the reaction schemes ranging from a small number of effective reactions to complex schemes involving many species. Because of the variability in coal properties, not only from plant to plant, but also from hour to hour, simpler schemes are often found to be adequate. These also have the advantage of limiting computational run times. For volatile combustion, the generalised eddy dissipation concept model is often found to be satisfactory, since it takes into account the critical aspects of turbulent mixing, micro-mixing and chemical kinetics. More sophisticated flamlet models should undoubtedly be more accurate, but the advantages can be outweighed by uncertainties in coal characterisation.

It has been found that char combustion is adequately represented by a diffusion-limited surface reaction model, or by a mixed kinetics/diffusion surface reaction rate model. As with devolatilisation, difficulties in characterisation and variability in properties limits the extent to

which additional model complexity achieves improved predictive capability in real industrial applications.

SO_x , NO_x, and soot emissions are of major environmental importance, and the ability to predict the amounts of these emissions can lead to furnace improvements that give better environmental performance. It is essential therefore to use sub-models for these species that capture all the critical sub-processes. Such sub-models have been published in the literature and used with some success (e.g. Li et al, 2004, Brown and Fletcher, 1998), but on-going experimental work is required to further refine the equations.

Slagging and fouling can have a major impact on furnace and boiler performance. A comprehensive model of such complicated phenomena has not yet been developed, but CFD modelling can nonetheless provide extremely valuable insights into slagging and fouling – their effects and how to minimise them. For example, the authors have investigated the sensitivity of the flue gas exit temperature (FGET) of the unit No. 3 at TRUenergy's Yallourn power plant to the thickness of a slagging layer.

In summary, CFD models for PC combustion have now been developed that provide adequately accurate prediction of furnace performance to be useful for the purposes of design and optimisation. On-going refinement of various sub-models will be necessary to improve predictive capability. This endeavour will require further experimental investigation of coal combustion sub-processes and improved characterisation additionally improved measurement techniques for collecting detailed data within operating furnaces will be needed. Further programs of the sort carried out by Tian et al. (2012) involving modelling of industrial furnaces together with industrial measurements for model validation are also necessary.

REFERENCES

Allardice D (2000) The utilisation of low rank coals. The Australian Coal Review 2000 October:40-46.

ANSYS/CFX (2015) ANSYS/CFX 16.0 Theory Guide. ANSYS, Inc. Canonsburg, USA,

ANSYS/FLUENT (2015) ANSYS FLUENT 16.0 User's Guide. ANSYS, Inc. Canonsburg, USA.

Backreedy R, Fletcher L, Ma L, Pourkashanian M, Williams A (2006) Modelling pulverised coal combustion using a detailed coal combustion model. Combust Sci Technol 178:763-787.

Backreedy R et al. (2005) Prediction of unburned carbon and NO x in a tangentially fired power station using single coals and blends. Fuel 84:2196-2203.

Basu P, Kefa C, Jestin L (1999) Boilers and burners: design and theory. Springer, New York,

Belosevic S, Sijercic M, Oka S, Tucakovic D (2006) Three-dimensional modeling of utility boiler pulverized coal tangentially fired furnace. Int J Heat Mass Transfer 49:3371-3378.

Benim A, Epple B, Krohmer B (2005) Modelling of pulverised coal combustion by a Eulerian-Eulerian two-phase flow formulation. Progr Comput Fluid Dynam Int J 5:345-361.
Bhambare KS, Ma Z, Lu P (2010) CFD modeling of MPS coal mill with moisture evaporation. Fuel Process Technol 91:566-571.
Boardman RD, Smoot LD (1993) Chapter 6 Pollutant Formation and Control
In: Smoot LD (ed) Fundamentals of Coal Combustion: For Clean and Efficient Use. Elsevier Science Publishers, The Netherlands,
BREE (2014) 2014 Australian Energy Update. Bureau of Resources and Energy Economics, Canberra
Brown AL, Fletcher TH (1998) Modeling soot derived from pulverized coal. Energy Fuels 12:745-757.
Chen L, Yong SZ, Ghoniem AF (2013) Modeling the slag behavior in three dimensional CFD simulation of a vertically-oriented oxy-coal combustor. Fuel Process Technol 112:106-117.
Díez LI, Cortés C, Pallarés J (2008) Numerical investigation of NO x emissions from a tangentially-fired utility boiler under conventional and overfire air operation. Fuel 87:1259-1269.
Duong TH (1985) Mathematical modelling of pulverised Victorian brown coal combustion and heat transfer in a plug-flow reactor. Proceedings of Third Australian Conference on Heat and Mass Transfer.
Duong TH (1987) Modelling of Brown Coal Combustion in One-dimension. NERDDP Project 931, End of grant Report, Report No ND/87/040. the State Electricity Commission of Victoria.
Edge P et al. (2011) Combustion modelling opportunities and challenges for oxy-coal carbon capture technology. Chem Eng Res Des 89:1470-1493.
EIA (2013) International Energy Outlook 2013. U.S. Energy Information Administration, Washington
Fan J, Qian L, Ma Y, Sun P, Cen K (2001) Computational modeling of pulverized coal combustion processes in tangentially fired furnaces. Chem Eng J 81:261-269.
Field MA, Gill DW, Morgan BB, Hawksley PGW (1967) Combustion of Pulverized Coal. BCURA, England:189–192.
Fiveland W, Wessel R (1988) Numerical model for predicting performance of three-dimensional pulverized-fuel fired furnaces. J Eng Gas Turbines Power 110:117-126.
German A, Mahmud T (2005) Modelling of non-premixed swirl burner flows using a Reynolds-stress turbulence closure. Fuel 84:583-594.
Gibb J (1985) Combustion of residual char remaining after devolatilization. Lecture at course of pulverized coal combustion Imperial College. Cited in ANSYS/CFX 16.0 Theory Guide. ANSYS, Inc. Canonsburg, USA.
Grant DM, Pugmire RJ, Fletcher TH, Kerstein AR (1989) Chemical model of coal devolatilization using percolation lattice statistics. Energy Fuels 3:175-186.
Hodges S, Holden J (2003) Impact of coal quality on power station performance. A continuing education course on the Science and Technology of Lignite Utilisation. CRC for Clean Power from Lignite, Melbourne.
IIBD (2002) Improving industrial burner design with computational fluid dynamics tools: Progress, Needs, and R&D Priorities. Workshop Report,
Jones J, Pourkashanian M, Williams A, Chakraborty R, Sykes J (1998) Modeling of coal combustion processes--A review of present status and future needs. Pittsburgh Coal Conference, Pittsburgh, PA (United States).
Jones JC, Stacy WO (1986) Devolatilization of Victorian brown coal. Part 2. Oxidizing conditions. R& D ReportND/86/025. State Electricity Commission of Victoria
Jovanovic R, Milewska A, Swiatkowski B, Goanta A, Spliethoff H (2012) Sensitivity analysis of different devolatilisation models on predicting ignition point position during pulverized coal combustion in O_2/N_2 and O_2/CO_2 atmospheres. Fuel 101:23-37.
Kiss LT, Brockway DJ, George AM, Stacy WO (1984) Properties of brown coals from the Rosedale, Stradbroke and Gormandale fields. SECV, Research and Development Department Report No SC/84/85,

Launder BE, Spalding D (1974) The numerical computation of turbulent flows. Comput Method Appl M 3:269-289.
Le Bris T, Cadavid F, Caillat S, Pietrzyk S, Blondin J, Baudoin B (2007) Coal combustion modelling of large power plant, for NOx abatement. Fuel 86:2213-2220.
Li K, Thompson S, Peng J (2004) Modelling and prediction of NO x emission in a coal-fired power generation plant. Control Eng Pract 12:707-723.
Lockwood F, Salooja A (1983) The prediction of some pulverized bituminous coal flames in a furnace. Combust Flame 54:23-32.
Magnussen BF, Hjertager B On the structure of turbulence and a generalized eddy dissipation concept for chemical reaction in turbulent flow. In: 19th AIAA Aerospace Meeting, St. Louis, USA, 1981.
Magnussen BF, Hjertager BH On mathematical modeling of turbulent combustion with special emphasis on soot formation and combustion. In: Symposium (International) on Combustion, 1977. vol 1. Elsevier, pp 719-729.
Menter FR (1992) Improved two-equation k-omega turbulence models for aerodynamic flows. NASA STI/Recon Technical Report N 93:22809.
Menter FR (1994) Two-equation eddy-viscosity turbulence models for engineering applications. AIAA J 32:1598-1605.
Mitchell RE (2000) An intrinsic kinetics-based, particle-population balance model for char oxidation during pulverized coal combustion. P Combust Inst 28:2261-2270.
Mulcahy M, Morley W, Smith I (1991) Combustion, gasification and oxidation. The Science of Victorian Brown Coal: Structure, Properties, and Consequences for Utilization:359.
Niksa S (1996) Coal combustion modelling vol 31. IEA Coal Research.
Ouyang S, Yeasmin H, Mathews J (1998) A pressurized drop-tube furnace for coal reactivity studies. Rev Sci Instrum 69:3036-3041.
Perera S, Faltsi-Saravelou O SOx Formation Model For Turbulent Combustion Applications. In: Third European Combustion Meeting ECM, 2007.
Roberts RA, Loveridge DJ (1969) Devolatilisation and combustion rate measurements on pulverised fuel particles of Morwell, Morwell Woody and Loy Yang coal. Document 4C/47, British Coal Utilisation Research Association
Sainsbury RB, Hawksley PGW (1969) Devolatilisation and combustion rate measurements on pulverised fuel particles of Yallourn Open Cut Coal. Combustion Note 825. British Coal Utilisation Research Association.
Saqr KM (2011) Comments on:“CFD analysis on the influence of helical carving in a vortex flow solar reactor” by N. Ozalp and D. JayaKrishna (Int. J. Hydrogen Energy 2010: 35, 6248–6260). Int J Hydrogen Energy 36:2320-2322.
Sazhin S, Sazhina E, Faltsi-Saravelou O, Wild P (1996) The P-1 model for thermal radiation transfer: advantages and limitations. Fuel 75:289-294.
Seggiani M (1998) Modelling and simulation of time varying slag flow in a Prenflo entrained-flow gasifier. Fuel 77:1611-1621.
Street PJ (1979) Single particle studies of brown coal combustion. CEGB Research Division Memorandum, MM/COMB, TH94.
Tian ZF, Nathan GJ, Cao Y (2015) Numerical modelling of flows in a Solar-Enhanced Vortex Gasifier: Part 1, Comparison of Turbulence Models. Progr Comput Fluid Dynam Int J 15:114-122.
Tian ZF, Tu JY, Yeoh GH (2005) Numerical simulation and validation of dilute gas-particle flow over a backward-facing step. Aerosol Sci Technol 39:319-332.
Tian ZF, Witt PJ, Schwarz MP, Yang W (2009) Comparison of two-equation turbulence models in simulation of a non-swirl coal flame in a pilot-scale furnace. Combust Sci Technol 181:954-983.
Tian ZF, Witt PJ, Schwarz MP, Yang W (2010a) Modeling Issues in CFD Simulation of Brown Coal Combustion in a Utility Furnace. J Compt Multiphase Flow 2:73-88.

Tian ZF, Witt PJ, Schwarz MP, Yang W (2010b) Numerical Modeling of Victorian Brown Coal Combustion in a Tangentially Fired Furnace. Energy Fuels 24:4971-4979.
Tian ZF, Witt PJ, Schwarz MP, Yang W (2012) Combustion of Predried Brown Coal in a Tangentially Fired Furnace under Different Operating Conditions. Energy Fuels 26:1044-1053.
Tian ZF, Witt PJ, Yang W, Schwarz MP (2011) Numerical simulation and validation of gas-particle rectangular jets in crossflow. Comput Chem Eng 35:595-605.
Tillman D (1991) The combustion of solid fuels and wastes. Academic Press.
Truelove J, Holcombe D Measurement and modelling of coal flame stability in a pilot-scale combustor. In: Symposium (International) on Combustion, 1991. vol 1. Elsevier, pp 963-971.
Vascellari M, Cau G (2012) Influence of turbulence–chemical interaction on CFD pulverized coal MILD combustion modeling. Fuel 101:90-101.
Versteeg HK, Malalasekera W (2007) An introduction to computational fluid dynamics: the finite volume method. Pearson Education.
Viskanta R, Mengüç M (1987) Radiation heat transfer in combustion systems. Prog Energy Combust Sci 13:97-160.
Visona S, Stanmore B (1998) Modelling NO formation in a swirling pulverized coal flame. Chem Eng Sci 53:2013-2027.
Wang X, Zhao D, He L, Jiang L, He Q, Chen Y (2007) Modeling of a coal-fired slagging combustor: Development of a slag submodel. Combust Flame 149:249-260.
Weber R, Peters A, Breithaupt P, Visser B (1995) Mathematical modeling of swirling flames of pulverized coal: what can combustion engineers expect from modeling? J Fluids Eng 117:289-297.
Weber R, Visser B, Boysan F (1990) Assessment of turbulence modeling for engineering prediction of swirling vortices in the near burner zone. Int J Heat Fluid Flow 11:225-235.
Wilcox DC (1988) Reassessment of the scale-determining equation for advanced turbulence models. AIAA J 26:1299-1310.
Williams A, Pourkshanian M, Jones JM, Skorupska N (2000) Combustion and Gasification of Coal. Taylor & Francis, New York, USA.
Wu Z (2005) Fundamentals of pulverised coal combustion. IEA Clean Coal Centre Reports
Xu M, Azevedo J, Carvalho M (2001) Modeling of a front wall fired utility boiler for different operating conditions. Comput Method Appl M 190:3581-3590.
Yeasmin H, Mathews J, Ouyang S (1999) Rapid devolatilisation of Yallourn brown coal at high pressures and temperatures. Fuel 78:11-24.
Yeoh GH, Yuen KK (2009) Computational fluid dynamics in fire engineering: Theory, modelling and practice. Butterworth-Heinemann.
Zhang J, Nieh S (1997) Comprehensive modelling of pulverized coal combustion in a vortex combustor. Fuel 76:123-131.
Zhou L, Li L, Li R, Zhang J (2002) Simulation of 3-D gas-particle flows and coal combustion in a tangentially fired furnace using a two-fluid-trajectory model. Powder Technol 125:226-233.